Available online at www.sciencedirect.com
ScienceDirect
International Journal of Solids and Structures 44 (2007) 1755–1767
INTERNATIONAL JOURNAL OF SOLIDS and STRUCTURES
www.elsevier.com/locate/ijsolstr

Thin film/substrate systems featuring arbitrary film thickness and misfit strain distributions. Part II: Experimental validation of the non-local stress/curvature relations

M.A. Brown [a], A.J. Rosakis [a], X. Feng [b,*], Y. Huang [b], Ersan Üstündag [c]

[a] *Graduate Aeronautical Laboratory, California Institute of Technology, Pasadena, CA 91125, USA*
[b] *Department of Mechanical and Industrial Engineering, University of Illinois, Urbana, IL 61801, USA*
[c] *Ames Laboratory and Department of Materials Science and Engineering, Iowa State University, Ames, IA 50011, USA*

Received 20 July 2006; received in revised form 10 October 2006
Available online 20 October 2006

Abstract

The classical Stoney formula relating local equibiaxial film stress to local equibiaxial substrate curvature is not well equipped to handle realistic cases where the film misfit strain, the plate system curvature, and the film thickness and resulting film stress vary with in-plane position. In Part I of this work we have extended the Stoney formula to cover arbitrarily non-uniform film thickness for a thin film/substrate system subject to non-uniform, isotropic misfit strains. The film stresses are found to depend non-locally on system curvatures. In Part II we have designed a demanding experiment whose purpose is to validate the new analysis for the case of radially symmetric deformations. To achieve this, a circular film island with sharp edges and a radially variable, but known, thickness is deposited on the wafer center. The plate system's curvatures and the film stress distribution are independently measured by using white beam and monochromatic X-ray microdiffraction (μXRD) measurements, respectively. The measured stress field (from monochromatic μXRD) is compared to the predictions of various stress/curvature analyses, all of which have the white beam μXRD measurements as input. The results reveal the shortcomings of the "local" Stoney approach and validate the accuracy of the new "non-local" relation, most notably near the film island edges where stress concentrations dominate.

Keywords: Thin film; X-ray microdiffraction; Non-local stress/curvature relations

1. Introduction and motivation

As the semiconductor industry develops ever smaller dimensions of thin metal film interconnections and more complex multilayered (film stack) structures, the mechanical properties and stresses of thin films used

* Corresponding author. Tel.: +1 2173335993.
E-mail address: xuefeng@uiuc.edu (X. Feng).

0020-7683/$ - see front matter © 2006 Elsevier Ltd. All rights reserved.
doi:10.1016/j.ijsolstr.2006.10.015

for these structures become major factors in controlling the reliability of integrated circuits (ICs). Thin film stress, as well as unintended stress non-uniformities, may cause cracking, buckling or even delamination, limiting applications of thin film technology. On the other hand, intentionally induced film stress in certain layers of a multilayered structure can be used to help control the properties of the entire stack. In such cases, ensuring stress uniformity and a prescribed constant stress level across the entire wafer becomes a goal of paramount importance. In either case, it is very important to be able to quantify the stress levels and to ensure stress uniformity in thin film structures deposited on large substrates.

Unfortunately, there is not a practical method to routinely measure film stress on large, 300 mm wafers directly after each of the many processing steps for the purpose of quality control. Furthermore, most available optical methods do not provide full-field (entire wafer) information. Stress in small thin film features can be measured using X-ray microdiffraction (μXRD). However, this highly accurate technique, which is very time-consuming, can only be practiced at certain national lab facilities and is not available to industry for routine measurements. Instead, the typical method of determining stress is through various wafer curvature techniques which calculate stress from measurements of the substrate wafer's shape through various equations relating film stress to substrate curvature changes.

The standard relation which infers film stress from substrate curvature changes is known as the Stoney formula. This relation describes a plate system composed of a stress-bearing thin film of uniform thickness h_f, deposited on a relatively thick substrate of uniform thickness h_s. The Stoney formula is a relation between the curvature change, $\kappa = \kappa_f - \kappa_i$, of the system and the stress, $\sigma^{(f)}$, of the film following a process. Before the process, the initial system curvature is κ_i, while after the process the final curvature is κ_f. This simple relation is given by:

$$\sigma^{(f)} = \frac{E_s h_s^2 \kappa}{6 h_f (1 - \nu_s)}. \tag{1.1}$$

The Stoney formula was derived based on standard plate theory subject to a large number of simplifying assumptions (Freund and Suresh, 2004), namely:

(i) Both the film thickness h_f and substrate thickness h_s are uniform, and the film and substrate have the same radius ($R_f = R_s$), and $h_f \ll h_s \ll R_s$;
(ii) The strains and rotations of the plate system are infinitesimal;
(iii) Both the film and substrate are homogeneous, isotropic, and the substrate is linearly elastic;
(iv) The film stress states are in-plane isotropic or equibiaxial (two equal stress components in any two, mutually orthogonal in-plane directions), while the out-of-plane direct stress and all shear stresses (in-plane and out-of-plane) vanish;
(v) The system's curvature components are equibiaxial (two equal direct curvatures) while the twist curvature vanishes in all directions; and
(vi) All surviving stress and curvature components are spatially constant over the plate system's surface, a situation which is often violated in practice.

When the formula is used, many of these constraints are routinely ignored. The formula has been expanded to relax many of the above listed assumptions (e.g., Freund and Suresh, 2004; Wikstrom et al., 1999a; Shen et al., 1996; Wikstrom et al., 1999b; Park and Suresh, 2000; Masters and Salamon, 1993; Salamon and Masters, 1995; Finot et al., 1997; Freund, 2000; Lee et al., 2001; Park et al., 2003). However, all of the above extensions still include the most restrictive of the assumptions, that of spatial uniformity, which does not allow the film stress, the film system or the system curvatures to vary across the plate surface. This crucial assumption is often violated in practice since spatial non-uniformities arising from various processing steps (e.g. deposition, annealing, etching, etc.) and from non-uniform film geometries across the wafer result in film stresses and the associated system curvatures that are non-uniformly distributed over the plate area. In order to address some of these important cases, Huang et al. (2005), Huang and Rosakis (2005), and Ngo et al. (2006) expanded the original formulation to describe films subject to non-uniform misfit strain or temperature distributions. The most important characteristic feature of these results is that the film stress components depend "non-locally"

on the substrate curvature components, i.e., that they depend on the curvature fields of the entire substrate and not only on the "local" value of the curvature components at the position where the stresses are to be estimated.

For the most recent part of this series of papers, Feng et al. (2006) relaxed part of assumption (i) to study thin film and substrate of different radii. Finally, Part I of this work further relaxed this assumption to study arbitrarily non-uniform thickness of the thin film. They derived a relation between the film stresses and the system curvatures which allows for the accurate experimental inference of film stress from full-field curvature measurements once the film thickness distribution is known.

In Part II of this study, two independent types of X-ray microdiffraction were used to measure both substrate slope and film stress across the diameter of an axisymmetric thin film – Si substrate specimen composed of a Si substrate on which a smaller circular W film island was deposited. The substrate slopes, measured by polychromatic (white beam) X-ray microdiffraction, were used to calculate curvature fields and to thus infer the film stress distribution using both the "local" Stoney formula and the new, non-local relation. The variable film thickness, which was independently measured, was also an input to the new relation. These were then compared with the film stress measured independently through monochromatic X-ray diffraction in the sample to both determine the validity of the new formula and to quantify the improvement over the established equation.

2. Specialization of the non-local stress/curvature relations of Part I to the case of radially symmetric variations

Consider a thin film of non-uniform, axisymmetric thickness $h_f(r)$ which is deposited on a circular substrate of constant thickness h_s and radius R_s, where r and θ are polar coordinates with an origin located at the geometrical center of the circular film/substrate system. The film is very thin, $h_f \ll h_s$, and is subject to axisymmetric misfit strain distribution $\varepsilon^m(r)$. The substrate is modeled as a plate since $h_s \ll R_s$. Young's modulus and Poisson's ratio of the film and substrate are denoted by E_f,v_f,E_s, and v_s, respectively.

The relation between film stress and system curvature for arbitrarily non-uniform misfit strain and film thickness has been given in Part I of this work (Ngo et al., 2006). In order to compare with the axisymmetric experimental data described in Sections 4 and 5, in Part II of this study we only consider the special case of axisymmetry (radial symmetry) and we provide relations between the film stress components ($\sigma_{rr}^{(f)}$ and $\sigma_{\theta\theta}^{(f)}$) and system curvature components (κ_{rr} and $\kappa_{\theta\theta}$) for the case of axisymmetric misfit strain and axisymmetric film thickness as follows:

$$\sigma_{rr}^{(f)}(r) - \sigma_{\theta\theta}^{(f)}(r) = -\frac{2E_f h_s}{3(1+v_f)}[\kappa_{rr}(r) - \kappa_{\theta\theta}(r)], \tag{2.1}$$

$$\sigma_{rr}^{(f)}(r) + \sigma_{\theta\theta}^{(f)}(r) = \frac{E_s h_s^2}{6h_f(r)(1-v_s)}\left[\kappa_{rr}(r) + \kappa_{\theta\theta}(r) + \frac{1-v_s}{1+v_s}(\kappa_{rr}(r) + \kappa_{\theta\theta}(r) - \overline{\kappa_{rr} + \kappa_{\theta\theta}})\right], \tag{2.2}$$

where $\overline{\kappa_{rr} + \kappa_{\theta\theta}} = \frac{1}{\pi R_s^2}\int\int_A [\kappa_{rr}(r) + \kappa_{\theta\theta}(r)]\,dA$ is the average curvature over the entire area A of the substrate. The above relations are special cases of Eqs. (4.4a) and (4.4c) of Part I for the case of radially varying stresses, curvatures, and film thickness. It is important to note that stresses at a point in the thin film depend not only on curvatures at that same point (local dependence), but also on the curvatures in the entire substrate (non-local dependence) via the average curvature $\overline{\kappa_{rr} + \kappa_{\theta\theta}}$. It is worthwhile to point out that the difference in normal stresses $\sigma_{rr}^{(f)} - \sigma_{\theta\theta}^{(f)}$ is independent of the thin film thickness h_f, but the sum of normal stresses $\sigma_{rr}^{(f)} + \sigma_{\theta\theta}^{(f)}$ is inversely proportional to the local film thickness h_f at that point. Finally, when the curvatures are uniform and isotropic ($\kappa_{rr} = \kappa_{\theta\theta}$) the equibiaxial, "local" form of the Stoney formula is recovered as a special case.

For non-uniform misfit strain distribution $\varepsilon^m = \varepsilon^m(r)$, the shear stress at the film/substrate interface does not vanish, and is denoted by τ_r. As shown in Eq. (4.4b) of Part I, for the case of arbitrary stress, curvature, and thickness variation, shear stresses also exist at the film/substrate interface. For the case of radial symmetry, the interface shear stress τ_r can also be directly related to substrate curvatures via

$$\tau_r = \frac{E_s h_s^2}{6(1-v_s^2)}\frac{d[\kappa_{rr}(r) + \kappa_{\theta\theta}(r)]}{dr}, \tag{2.3}$$

which is also independent of the film thickness h_f. Eq. (2.3) provides a way to determine the interfacial shear stresses from the gradients of substrate curvatures. For the special case of uniform curvatures across the plate, Eq. (2.3) predicts no interfacial shear stresses between the film and substrate, as assumed by the Stoney formula.

To verify these equations, both the slope and film stress across the diameter of an axisymmetric specimen were measured using X-ray microdiffraction. The substrate slope obtained by white beam μXRD was differentiated to calculate the two curvature components κ_{rr} and $\kappa_{\theta\theta}$. These were then used to calculate film stress through Eqs. (2.1), (2.2), (2.3), which was compared with both the stress determined from the Stoney formula and the stress measured by monochromatic μXRD.

3. X-ray microdiffraction (μXRD)

X-ray microdiffraction is a local strain measurement technique which, in general, uses the change in lattice spacing in a crystalline structure as a local micro-strain gage. The incoming beam diffracts from the crystalline lattice to form Laue patterns, which can be analyzed to measure the sample strain. Stress is subsequently calculated by assuming elasticity and specific values of the material's elastic constants. Synchrotron radiation was used in this experiment to utilize its very small beam size ($\sim 1 \times 1$ μm), high energy, and ability to use either a monochromatic or a polychromatic (white) X-ray beam. If used in the white beam mode, μXRD can also function as a micro-rotation gage to obtain information about lattice rotation.

3.1. White beam μXRD

Laue patterns from a white beam form Laue spots (Fig. 1a), where each spot is generated by a specific X-ray energy selected by a given lattice plane. A sophisticated software program then deconvolutes these patterns and indexes them; identifying individual patterns from each grain (Tamura et al., 2003). From this analysis, one can determine the orientation matrix of each grain as well as its deviatoric strain. (The deviatoric stress is then found using Hooke's law (Noyan and Cohen, 1987).) When there are too many grains in an image, the software is unable to determine which spots correspond to which grains, and cannot analyze the image. Therefore, white X-rays are used when the grain size is comparable to or larger than the beam size.

In the case of a single crystal specimen, the measured orientation matrix is always from the same grain. Once the crystal orientation is obtained at each location across the specimen, the relative slope and curvature are determined by tracking the changes in the vector defining the grain normal with respect to an arbitrarily set lab coordinate system. For a scan along the x axis (sample diameter), we are only concerned with the slope changes in the xz plane. This slope is equal to $\tan(\alpha)$, where α is defined as the angle between the projection of the grain normal in the xz plane and the z axis in the lab reference frame (Fig. 1b).

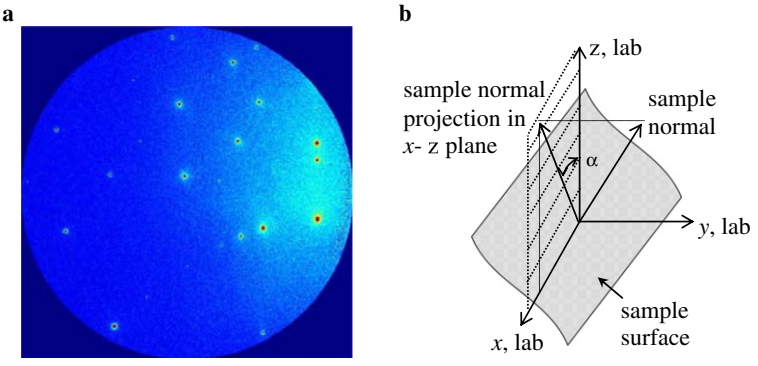

Fig. 1. (a) Laue pattern from the single crystal Si wafer. (b) Definition of coordinate system and the projection angle α; slope in xz plane $= \tan(\alpha)$.

For a radially symmetric sample on which the scan is performed along the diameter, where $y = 0$, cylindrical coordinates can be used. The radial slope is given by $\partial f/\partial r = \tan(\alpha)$, and the circumferential curvatures κ_{rr} and $\kappa_{\theta\theta}$ are then determined from

$$\kappa_{rr} = \frac{\partial^2 f}{\partial r^2} = \frac{\partial(\tan\alpha)}{\partial r}, \tag{3.1}$$

$$\kappa_{\theta\theta} = \frac{1}{r}\frac{\partial f}{\partial r} = \frac{1}{r}(\tan\alpha). \tag{3.2}$$

3.2. Monochromatic μXRD

When dealing with a film whose grains are much smaller than the beam spot size, a white beam cannot be used. In this case, the average equibiaxial stress ($\sigma_{xx} = \sigma_{yy} = \sigma$, $\sigma_{xy} = 0$) can be measured with monochromatic X-rays. Laue patterns from a monochromatic beam form Debye rings in ψ-2θ spatial coordinates (Fig. 2).

The average equibiaxial film stress is found using what is known as the "d vs $\sin^2\psi$" method (Noyan and Cohen, 1987). With this method, 2θ vs ψ is first graphed to find the intercept, i.e., θ at $\psi = 0$, or θ_0. Next the well-known Bragg's law ($\lambda = 2d\sin\theta$, where λ is the monochromatic beam wavelength) is used to find the lattice spacing, d, from the 2θ peaks, and then d vs $\sin^2\psi$ is plotted to find its slope, s. This slope, s; d_0 (d at θ_0); and the material constants are input into the equation for the equibiaxial stress (Noyan and Cohen, 1987)

$$\frac{d - d_0}{d_0} = \frac{1+v}{E}\sigma\sin^2\psi - \frac{2v}{E}\sigma \tag{3.3}$$

to find the stress, σ, as

$$\sigma = \frac{E * \text{slope}}{(1+v)d_0}. \tag{3.4}$$

If the stress is not actually equibiaxial, then Eq. 3.4 refers to the mean stress, $\sigma = (\sigma_{xx} + \sigma_{yy})/2$.

The experiments described in the following sections were performed at beamline 7.3.3 at the Advanced Light Source (ALS) at Lawrence Berkeley National Laboratory in Berkeley, CA. This beamline is able to quickly switch between white and monochromatic X-rays, in order to measure substrate curvature and film stress, respectively, at the same location on the sample. The reflection X-ray setup is shown in Fig. 3.

4. Experimental procedure and specimen specifications

The specimen consisted of a circular, 24.8 mm diameter circular W film island deposited on the center of a 100 mm diameter, 525 μm thick Si 001 wafer (Fig. 4). The film thickness is variable across the island; the thickest portion, in the center of the island, is approximately 1.85 μm. Young's modulus for Si and W are 130 and 410 GPa, respectively, while Poisson's ratio is 0.28 for both materials (Gouldstone et al., 1998).

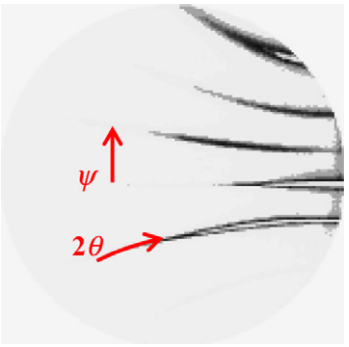

Fig. 2. Monochromatic beam (8 keV) diffraction patterns from a W thin film on Si substrate.

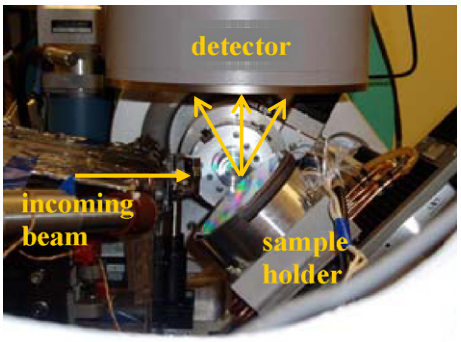

Fig. 3. The microdiffraction setup at the Advanced Light Source. The incoming X-ray beam is reflected from the sample surface and captured by the detector.

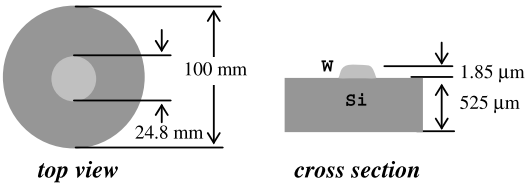

Fig. 4. Sample schematic.

Coherent gradient sensing (CGS), an optical curvature measurement technique (Rosakis et al., 1998), was used to find the topography of the specimen (Fig. 5). As expected from the geometry, the shape is axisymmetric, resembling a straw hat. It has a fairly constant, negative curvature under the film island, a non-zero, positive curvature in the area of bare Si, and features a radial curvature jump between the two regions. Preliminary optical data for this configuration have been reported by Brown et al. (2006).

As evident from Fig. 5b, the full-field wafer shape measurement clearly reveals the non-local nature of the stress/curvature dependence in this system. Indeed, the figure shows that even at points on the wafer which are not covered by any film (points outside the island), the curvature is still non-zero. This is contrary to the predictions of the Stoney formula, which uniquely relates "local" curvature to "local" membrane stress (zero for these areas), and demonstrates that the Stoney stress/curvature relation is, in concept, inadequate for analyzing the stress on the film-covered part of the wafer. Indeed, this observation provides a simple physical way to visualize the need of relaxing the uniformity (thickness, misfit strain, curvature, stress) assumptions that have resulted in the simple, but highly inadequate, Stoney relation. In the following sections we will use the ideal-

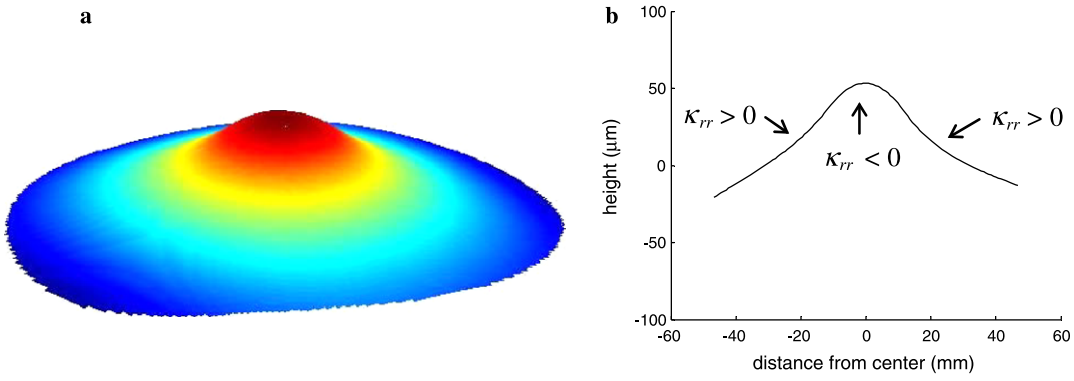

Fig. 5. Wafer topography, (a) full-field and (b) across the sample diameter.

ized substrate/film island system to quantify these issues. The geometry involving an island of finite diameter which is smaller than the substrate diameter provides a simple configuration through which the effect of film thickness variation and edge discontinuity can test the limits of the newly developed stress/curvature formulation of Part I.

A series of polychromatic (white beam) X-ray measurements were taken along the sample diameter, with a spacing of 0.1 mm, to find the sample slope ($\partial f/\partial x$). Due to the axisymmetric nature of the specimen ($\partial f/\partial x = \partial f/\partial r$), this single linear set of slope measurements across the sample diameter ($y = 0$) can be extrapolated to form full-field maps of both $\kappa_{rr}(r)$ and $\kappa_{\theta\theta}(r)$. These are subsequently used in conjunction with Eqs. (2.1)–(2.3) to infer the film stress across the island diameter. Full-field maps of both curvature components are necessary because of the non-local nature of Eqs. (2.2) and (2.3).

Monochromatic X-ray microdiffraction measurements were also taken along the island diameter, with a data point spacing of 0.25 mm, to separately measure the equibiaxial film stress along the same line ($y = 0$). This was compared with the stress determined from the equations. It is important to note that the μXRD slope and stress measurements use two different types of diffraction, and are therefore completely independent measurements of the sample state. Therefore, using slope measurements to infer the stress state through various stress/curvature relations and then to compare the results with the directly measured stress state, provides a legitimate way of evaluating and ultimately validating the newly proposed non-local stress/curvature equations.

Since variable thickness is a necessary input to these equations, the film thickness was also measured using a scanning electron microscope (SEM). Images of the film cross-section were taken in many locations along the film radius. Since the specimen topography is axisymmetric, the thickness across the island diameter was extrapolated from these measurements. In each image, the film thickness was determined by comparing the length of a line drawn through the thickness to the length of the scale bar (Fig. 6a and b). Each image covers approximately 8 μm, and five measurements within each image are averaged to obtain the film thickness at that particular measurement point. The film thickness variation with radial position is shown in Fig. 6c. Near the island edge, the thickness drops off precipitously from an approximate level of 1.85 μm in the center to approximately 0.8 μm at the edge of the island. From Eq. (2.2), this is expected to correspond with a rapid increase in film stress in that location.

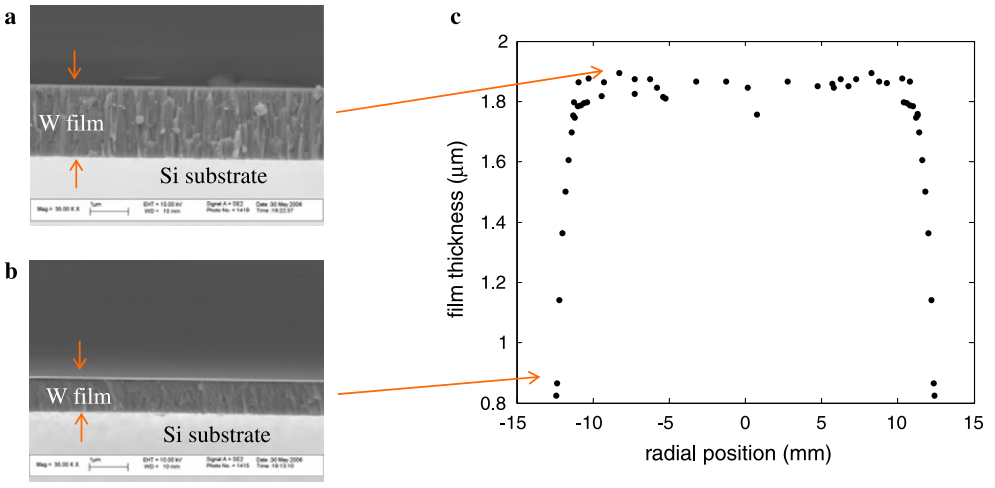

Fig. 6. SEM images of film cross-section (a) within the central approximately constant thickness region and (b) near the film edge; (c) radial film thickness measured from the SEM images.

5. X-ray microdiffraction (μXRD) results

5.1. White beam μXRD measurement

The radial slope, $\partial f/\partial r$, is shown in Fig. 7a. In the central part of the film-covered region of the wafer the slope appears to be approximately linear, but it substantially deviates from linearity as the film edges are approached from within. At the film edges, the radial gradient of the slope (radial curvature κ_{rr}) suffers a large but finite jump and changes sign (from negative to positive), consistent with the topography map of Fig. 6c. As the wafer edges are approached, the radial curvature decreases gradually to a small but finite value. The overall shape of the radial slope is anti-symmetric about the wafer origin, as would be expected from the shape axisymmetry. To conclusively demonstrate this, the data from one side was reflected about the origin and overlayed on the data of the other side. This exercise, shown here in Fig. 7b, demonstrates that the reflected slopes from either side agree to within 5%.

Since the specimen geometry, shape measured by CGS, and slope measured by XRD all suggest radial symmetry, the linear slope measurement from μXRD is used to construct full-field slope data. Indeed, the slope can now be replaced by two piecewise fits of two polynomials, one taken within the film portion and another outside it. Fig. 8 shows the high quality of the polynomial fits of the raw μXRD slope data. It should be noted that the two polynomial fits are required to pass through the same point corresponding to the estimated location of the film edge.

Fig. 9 shows the curvature distribution obtained when the polynomial fit of the slope, shown in Fig. 8, was used to determine the two independent wafer curvature components through Eqs. (3.1) and (3.2). The curvature $\kappa_{\theta\theta}$ is continuous across the film boundary, but the curvature κ_{rr} suffers a finite jump at the island edges. This is consistent with the observation of Brown et al. (2006). What is perhaps more interesting is that even within the area of coverage, both curvature components vary with radial position.

By further invoking axisymmetry, we may also use the film thickness measurement conducted along the island radius (Section 3) to construct the island thickness profile in place of full-field thickness data. The film thickness is then denoted by $h_f = h_f(r)$, and can be fit by the following radial distribution:

$$h_f = 1.85 + 0.00713\left(1 + \frac{1.49}{r - 12.6}\right)(r - 5.82)^2 H(r - 5.82), \quad r \leqslant R_f = 12.4\ \text{mm}, \tag{5.1}$$

where the radius r is in millimeters, the film thickness h_f is in micrometers, and H is the Heaviside step function. Fig. 10 compares Eq. (5.1) with the actual SEM thickness data and demonstrates their good agreement.

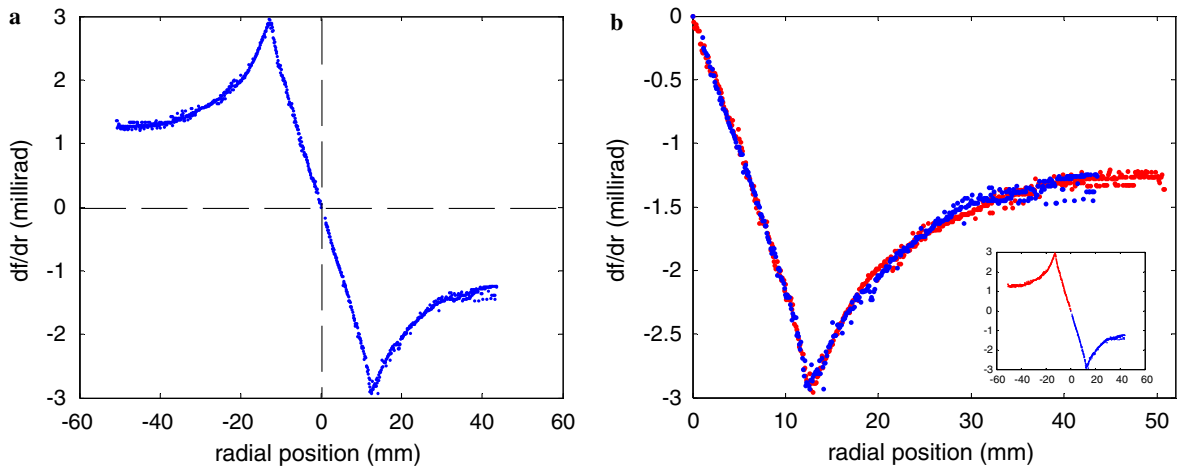

Fig. 7. (a) Slope along the sample diameter. (b) Slope from the center, overlapped, to show antisymmetry.

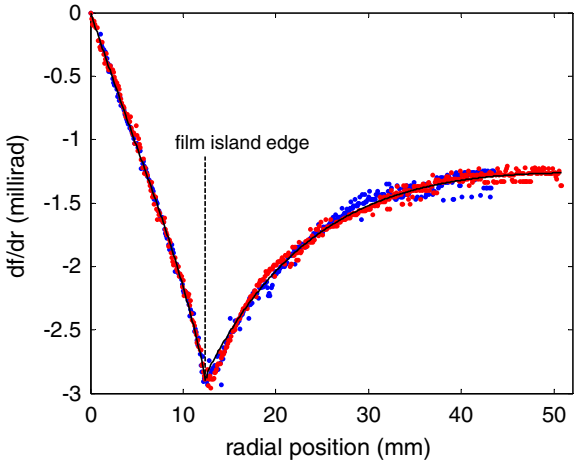

Fig. 8. Polynomial fit of XRD slope data.

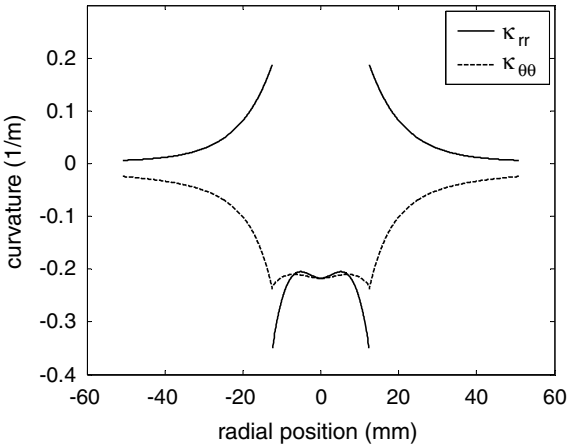

Fig. 9. Curvatures (κ_{rr} and $\kappa_{\theta\theta}$) obtained from the polynomial fit of white beam μXRD slope data from Eqs. (3.1) and (3.2).

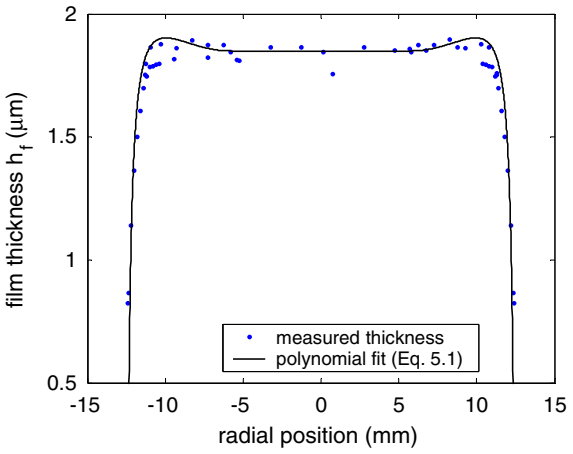

Fig. 10. Polynomial fit of thickness data.

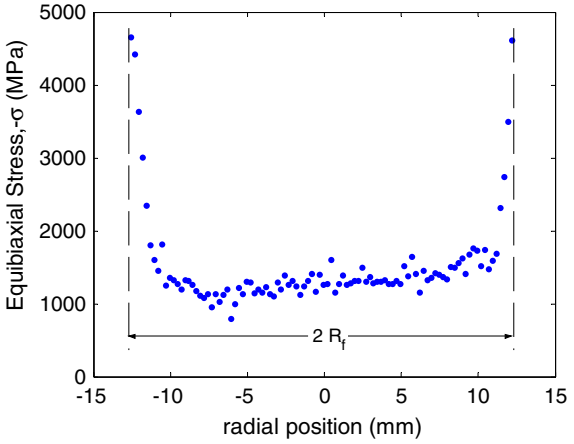

Fig. 11. Average equibiaxial film stress from monochromatic X-ray measurement.

5.2. Monochromatic μXRD measurement

The absolute magnitude of the mean stress, $-(\sigma_{rr}+\sigma_{\theta\theta})/2$, obtained through the monochromatic μXRD measurement is shown in Fig. 11. [Although the mean stress itself is compressive, we have decided to display its absolute magnitude for reasons of clarity of discussion.] The stress is approximately constant throughout most of the island diameter. However, near the island edge the stress increases very steeply to over five times its central value within a small (~2 mm) boundary layer from the film edge. This is clearly due to the existence of a strong thickness gradient near this edge (Fig. 6c). It is also due to the eventual existence of a traction-free boundary at the end of the film. These two geometrical effects, which result in a substantial stress concentration gradient (huge stresses developing from 1 to 5 GPa over a few millimeters of length[1]), provide a substantial prediction challenge to any theoretical model used for the inference of stress through substrate curvature measurements. In the following sections, we will concentrate on the ability of various techniques to independently predict this stress concentration.

6. Validation of the non-local stress/curvature model and conclusions

In this section we compare the results of the mean film stress distribution obtained through the monochromatic μXRD measurement with the stress distributions predicted via the use of three different theoretical stress/curvature models, one local (Stoney) and two non-local. The common input to these relations is the substrate curvatures (see Fig. 9) obtained through the independent white beam μXRD substrate slope measurement.

Fig. 12 illustrates this comparison. The discrete points are the stress distribution results of the direct monochromatic beam μXRD measurement. The dotted line shows the prediction of the Stoney equation (Eq. 1.1) with $\kappa(r)=[\kappa_{rr}(r)+\kappa_{\theta\theta}(r)]/2$ and $\sigma(r)=[\sigma_{rr}(r)+\sigma_{\theta\theta}(r)]/2$ being the mean stress and curvature, respectively. The Stoney relation assumes that the radius of the film, R_f, and that of the substrate, R_s, are equal and that the film thickness is uniform. Although the Stoney equation was derived strictly for constant κ and σ, it is used here in a local sense in which $\kappa(r)$ as measured (Fig. 9) is input into Eq. (1.1) to obtain the dotted stress distribution shown. The Stoney prediction underestimates the discrete stress data by as much as 50% in the central portion of the film and completely misses the dramatic 500% stress increase at the edges.

The dashed line shows a prediction of a non-local model in which the island film radius is different from the substrate radius ($R_s > R_f$) but the film thickness inside the island is assumed to be constant. The stresses are

[1] The yield stress of tungsten is around 1.5 GPa (Dummer et al., 1998; Maloy et al., 2005) such that the deformation of tungsten thin film is elastic except near the edge. The stress around the edge is very high to trigger film/substrate interface delamination, as to be discussed in the next section.

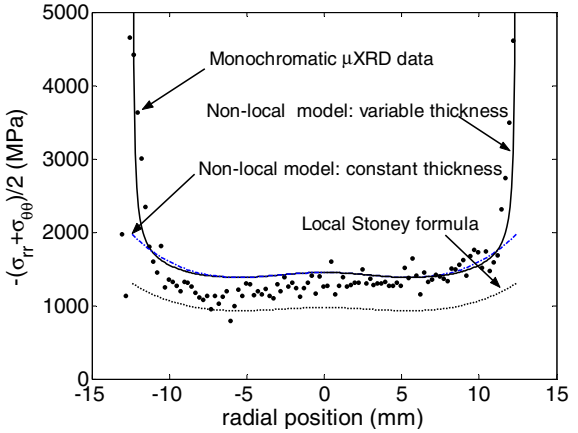

Fig. 12. Monochromatic μXRD stress data compared with calculated stress.

obtained by using Eq. (2.2), specialized to the case of constant film thickness $h_f = 1.85$ μm (approximate film thickness measured at the island center). This is still a non-local calculation since it also involves averaging the curvature field over the entire wafer to obtain $\overline{\kappa_{rr} + \kappa_{\theta\theta}}$. Howerver, it does not take into account the drastic reduction of the film thickness over a distance of a few millimeters from the edge (see Fig. 6). As is obvious from Fig. 12, this prediction approaches the discrete monochromatic μXRD measurement much better than the result based on Stoney, but still completely misses the severe stress concentration near the film edges.

Finally, the solid line represents the result of utilizing Eq. (2.2) in its most general form, in which thickness and curvatures are both allowed to vary with radial position r. The radial profile of the island film thickness $h_f(r)$ of Eq. (5.1) was used as input in this calculation. It is evident from Fig. 12 that this last calculation, utilizing the most general non-local relation, agrees very well with the monochromatic μXRD stress measurement over the entire film diameter, including the region close to the film edge. In particular, the success of the generalized non-local stress/curvature relation in capturing the dramatic stress increase that has been independently measured provides validation to the generalized analysis presented in Part I of this study.

An important byproduct of this analysis is its ability to also estimate interfacial shear stresses acting between the film and the substrate. These shear stresses are a direct consequence of in-plane non-uniformities. For our radially symmetric experiment, the only surviving shear stress, τ_r, is given by Eq. (2.3) and can readily be evaluated by differentiating $\kappa_{rr}(r) + \kappa_{\theta\theta}(r)$ of Fig. 9. This interfacial shear stress, shown here in Fig. 13, is not nearly as large as the direct film stress, but it climbs to approximately 400 MPa near the film edges. The combined presence of huge direct film stresses ($\sigma \sim 5$ GPa)[2] at the film edge and substantial interfacial shears may be enough to trigger interfacial delamination (Freund and Suresh, 2003). In fact, careful scrutiny of the film/substrate adhesion through SEM has revealed a well-defined and perfectly circular delamination front surrounding the island at $R_f \sim 12.4$ mm, very close to its edge. A local, SEM, view of this delamination is shown in Fig. 14.

The maximum in-plane shear stress $(\sigma^f_{rr} - \sigma^f_{\theta\theta})/2$ can also be calculated from Eq. (2.1) and from the curvature distributions (Fig. 9) obtained through the white beam μXRD measurement. The in-plane shear stress distribution across the island is shown in Fig. 15. We note that the maximum absolute value of this stress is less than 7 MPa or 0.2% of the in-plane mean stress. This suggests that for the present experiment the film stress state is, to all practical purposes, equibiaxial. This fact justifies the assumptions of equibiaxiality used in the analysis of the monochromatic μXRD measurement.

The analysis presented in Part I of this work provides a new formulation to infer film stresses in the presence of arbitrary non-uniformities in both thickness and misfit strain. In Part II, we demonstrate the necessity

[2] The direct stress of 5 GPa is clearly larger than the yield stress (around 1.5 GPa) of tungsten. But the domain of this large stress near the edge is very small. The inelastic behavior is not accounted for in the present study.

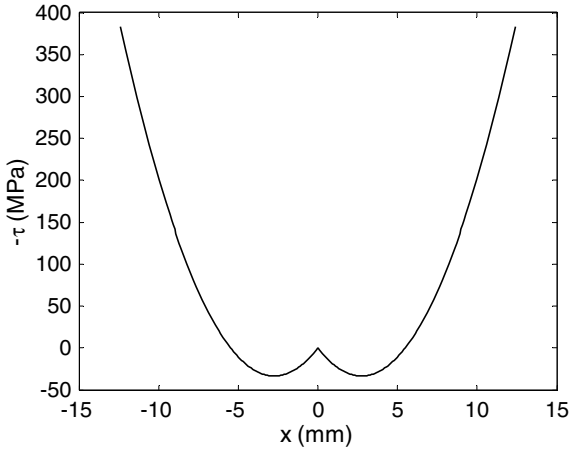

Fig. 13. Interface shear stress.

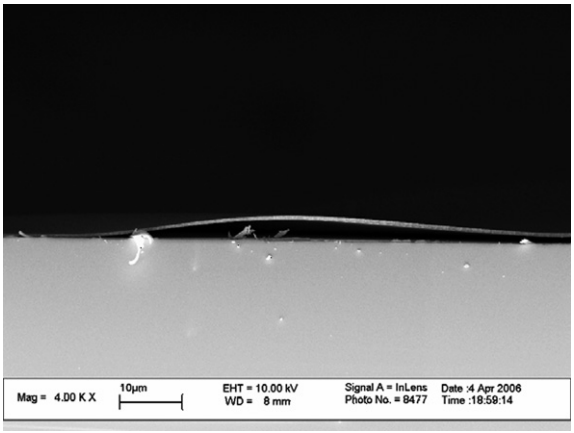

Fig. 14. Interface delamination observed via SEM near the film island edge.

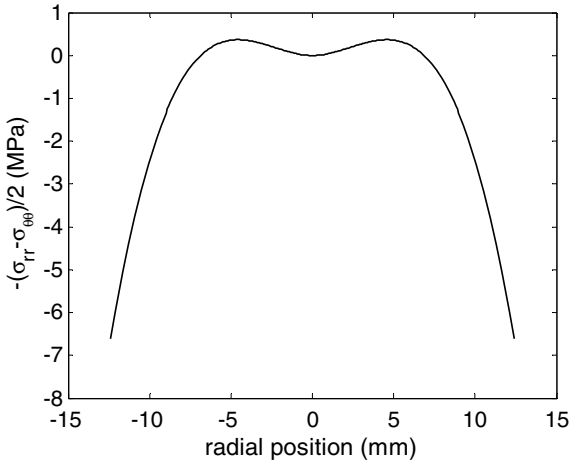

Fig. 15. In-plane shear stress.

of a non-local full-field curvature measurement approach, and we conclusively validate the theoretical model through comparison with an experiment featuring very high film stress gradients.

Acknowledgements

The Advanced Light Source is supported by the Director, Office of Science, Office of Basic Energy Sciences, Materials Sciences Division of the U.S. Department of Energy under Contract No. DE-AC03-76SF0098 at Lawrence Berkeley National Laboratory.

References

Brown, M.A., Park, T.S., Rosakis, A.J., Ustundag, E., Tamura, N., Valek, B., 2006. A comparison of x-ray microdiffraction and coherent gradient sensing in measuring discontinuous curvatures in thin film – substrate systems. J. Appl. Mech. (in press).

Dummer, T., Lasalvia, J.C., Ravichandran, G., Meyers, M.A., 1998. Effect of strain rate on plastic flow and failure in polycrystalline tungsten. Acta Mater. 46 (17), 6267–6290.

Feng, X., Huang, Y., Jiang, H., Ngo, D., Rosakis, A.J., 2006. The effect of thin film/substrate radii on the Stoney formula for thin film/substrate subjected to non-uniform axisymmetric misfit strain and temperature. J. Mech. Mater. Struct. (in press).

Finot, M., Blech, I.A., Suresh, S., Fijimoto, H., 1997. Large deformation and geometric instability of substrates with thin-film deposits. J. Appl. Phys. 81, 3457–3464.

Freund, L.B., 2000. Substrate curvature due to thin film mismatch strain in the nonlinear deformation range. J. Mech. Phys. Solids 48, 1159.

Freund, L.B., Suresh, S., 2004. Thin Film Materials: Stress, Defect Formation and Surface Evolution. Cambridge University Press, Cambridge.

Gouldstone, A., Shen, Y.-L., Suresh, S., Thompson, C.V., 1998. Evolution of stresses in passivated and unpassivated metal interconnects. J. Mater. Res. 13 (7), 1956–1966.

Huang, Y., Rosakis, A.J., 2005. Extension of Stoney's Formula to non-uniform temperature distributions in thin film/substrate systems. The case of radial symmetry. J. Mech. Phys. Solids 53, 2483–2500.

Huang, Y., Ngo, D., Rosakis, A.J., 2005. Non-uniform, axisymmetric misfit strain: in thin films bonded on plate substrates/substrate systems: the relation between non-uniform film stresses and system curvatures. Acta Mech. Sinica 21, 362–370.

Lee, H., Rosakis, A.J., Freund, L.B., 2001. Full-field optical measurement of curvatures in ultra-thin-film-substrate systems in the range of geometrically nonlinear deformations. J. Appl. Phys. 89 (11), 6116–6129.

Maloy, S.A., James, M.R., Sommer, W., Willcutt, G.J., Lopez, M., Romero, T.J., Toloczko, M.B., 2005. The effect of 800 MeV proton irradiation on the mechanical properties of tungsten at room temperature and at 475 degrees. J. Nucl. Mater. 343 (1–3), 219–226.

Masters, C.B., Salamon, N.J., 1993. Geometrically nonlinear stress–deflection relations for thin film/substrate systems. Int. J. Engr. Sci. 31, 915–925.

Ngo, D., Huang, Y., Rosakis, A.J., Feng, X., 2006. Spatially non-uniform, isotropic misfit strain in thin films bonded on plate substrates: the relation between non-uniform film stresses and system curvatures. Thin Solid Films (in press).

Noyan, I.C., Cohen, J.B., 1987. Residual Stress. Springer-Verlag, New York, Chapter 5.

Park, T.S., Suresh, S., 2000. Effects of line and passivation geometry on curvature evolution during processing and thermal cycling in copper interconnect lines. Acta Mater. 48, 3169–3175.

Park, T.S., Suresh, S., Rosakis, A.J., Ryu, J., 2003. Measurement of full-field curvature and geometrical instability of thin film-substrate systems through CGS interferometry. J. Mech. Phys. Solids 51 (11–12), 2191–2211.

Rosakis, A.J., Singh, R.P., Tsuji, Y., Kolawa, E., Moore Jr., N.R., 1998. Full-field measurements of curvature using coherent gradient sensing: application to thin film characterization. Thin Solid Films 325 (1–2), 42–54.

Salamon, N.J., Masters, C.B., 1995. Bifurcation in isotropic thin film/substrate plates. Int. J. Solids Struct. 32, 473–481.

Shen, Y.L., Suresh, S., Blech, I.A., 1996. Stresses, curvatures, and shape changes arising from patterned lines on silicon wafers. J. Appl. Phys. 80, 1388–1398.

Tamura, N., MacDowell, A.A., Spolenak, R., Valek, B.C., Bravman, J.C., Brown, W.L., Celestre, R.S., Padmore, H.A., Batterman, B.W., Patel, J.R., 2003. Scanning X-ray microdiffraction with submicrometer white beam for strain/stress and orientation mapping in thin films. J. Synchrotron Radiat. 10, 137–143.

Wikstrom, A., Gudmundson, P., Suresh, S., 1999a. Thermoelastic analysis of periodic thin lines deposited on a substrate. J. Mech. Phys. Solids 47, 1113–1130.

Wikstrom, A., Gudmundson, P., Suresh, S., 1999b. Analysis of average thermal stresses in passivated metal interconnects. J. Appl. Phys. 86, 6088–6095.